Journal of Materials Chemistry B

Accepted Manuscript

ROYAL SOCIETY OF CHEMISTRY

www.rsc.org/materialsB

Controlling aminosilane layer thickness to extend plasma half-life of stealth persistent luminescence nanoparticles *in vivo*

Thomas Maldiney,[a] *Maxime Rémond,*[a] *Michel Bessodes,*[a] *Daniel Scherman,*[a] *Cyrille Richard,*[a,*]

[a] Unité de Technologies Chimiques et Biologiques pour la Santé (UTCBS), CNRS UMR 8258, INSERM U 1022, Paris, F-75270 cedex France; Université Paris Descartes, Sorbonne Paris Cité, Faculté des Sciences Pharmaceutiques et Biologiques, Paris, F-75270 cedex France; ENSCP, Paris, F-75231 cedex France.

cyrille.richard@parisdescartes.fr

ABSTRACT. Therapeutic and diagnostics both initiated the development and rational design of nanoparticles intended for biomedical applications. Yet, the fate of these nanosystems *in vivo* is hardly manageable and generally results in their rapid uptake by the mononuclear phagocyte system, i.e. liver and spleen. To overcome this essential limitation, efforts have been made to understand the influence of physico-chemical parameters on the behaviour of nanoparticles *in vivo* and on their ability to be uptaken by phagocytic cells. Notably, polyethylene glycol grafting and precise control of its density have not only been shown to prevent protein adsorption on the surface of nanoparticles, but also to significantly reduce macrophage uptake *in vitro*. In this article, we suggest the use of persistent luminescence to study the influence of another parameter, aminosilane layer thickness, on both *in vitro* protein adsorption and *in vivo* biodistribution of stealth persistent nanophosphors.

KEYWORDS. Persistent luminescence, Nanoparticle, Aminosilane, PEG, Optical Imaging, In vivo, Biodistribution.

Introduction. The field of innovative nanotechnology steadily raises promising perspectives and adaptive tools intended for biological research and future medical applications.[1] Notably, attentions have increasingly focused on the rational design of nanoparticles to introduce novel solutions for the efficient diagnosis[2] and treatment of cancer.[3] Along with the development of such highly sophisticated nanocarriers, appeared the absolute necessity to understand their biological behavior in complex environment.[4] In particular, widespread preclinical studies *in vivo* unraveled the difficult task to control the biodistribution of nanoparticles following intravenous injection in living animals, whose physiological path through systemic circulation generally leads to a rapid sequestration by macrophages from the mononuclear phagocyte system (MPS), also referred to as the reticuloendothelial system (RES).[5,6,7]

Such recognition process is mainly associated with the "biological identity" acquired by a nanoparticle following the interaction with opsonins from the blood that decorate its surface and finally constitute a protein "corona", partly responsible for the biological fate of the particle.[8,9,10] Polyethylene glycol (PEG) grafting was first erected as "clocking" strategy to hinder the formation of this "corona" by creating a thermodynamic barrier to protein diffusion.[11] Consequently, increasing PEG density or chain length on the surface of a nanoparticle was shown to significantly slow down the uptake process by macrophages from the MPS.[12,13,14] Indeed, PEG grafting is usually required to achieve biocompatibility in nanoparticulate systems and effectively counter phagocytosis. However, PEG chains typically need to have a molecular weight higher than 2,000 Da which is generally responsible for a significant increase in hydrodynamic diameter and a clear tendency to aggregate under high salt conditions. In addition to this first method based on the use of PEG polymers, or hybrid PEG-copolymer derivatives,[15] several other strategies have already been envisioned to circumvent this problematic RES uptake. Among them, optimization of shape[16] and surface charge[17] of the nanoparticles were not only shown to enhance blood

circulation time, but also to limit the global sequestration within RES organs. To this end, zwitterionic coatings were recently introduced as a promising method to suppress the non specific adsorption of various biomolecules on a wide variety of different nanoparticles, providing an efficient way to circumvent the MPS system.[18] Likewise, the technique of layer-by-layer assembly was used to successfully stabilize and control the biodistribution of Quantum Dots (QDs) *in vivo*, leading to multilayer nanoparticles with long blood elimination half-life as well as low accumulation in the liver.[19] Yet, the prerogative to finally reach a proper understanding of such elaborated biological phenomenon as nanoparticles opsonization or biodistribution generally relies in the necessity to work with a reliable probe that returns accurate information with the best sensitivity.

To this end, we have previously reported the use of persistent luminescence nanoparticles (PLNP) as highly sensitive optical nanoprobes *in vivo* to naturally avoid the autofluorescence from biological tissues.[7,20] Surface functionalization was shown to enable efficient targeting of these PLNP to malignant cells *in vitro*,[21,22] as well as enhanced blood half-life for *in vivo* applications.[23] However, despite such promising characteristics, persistent luminescence could not be followed more than two hours in living animals, which impeded long-term applications.[24] We have recently overcome this essential limitation by introducing novel persistent luminescence nanoparticles, with formula $ZnGa_{1.995}Cr_{0.005}O_4$, which could be activated with low energy photons, in the therapeutic window, through living tissues.[25,26,27,28]

The present article employs this new generation of persistent luminescence nanoparticles to better understand the way surface functionalization affects the accumulation kinetics within major RES organs and blood half-life of ZGO nanoparticles. In particular, we focused our attention on the effect of aminosilane polycondensation and layer formation on the surface of the particle, showing that a significant increase in the silane layer thickness, prior to PEG grafting and at the expense of hydrodynamic diameter, is responsible for a far better circulation of the probe associated with a delayed RES uptake. This result not only raises additional information in the understanding of nanoparticles biological fate, but also opens alternatives to several biomedical applications that require long-circulating nanoprobes.

Results and discussion. Persistent luminescence nanoparticles with formula $ZnGa_{1,995}Cr_{0.005}O_4$, referrerd to as ZGO, were synthesized by a two-step method combining a hydrothermal treatment and a low-temperature sintering in air at 750°C for 5 hours. The diffraction pattern of ZGO powder confirms the formation of pure zinc gallate from cubic spinel phase (Supplementary Fig. S1.a). The introduction of trivalent chromium in this spinel lattice is responsible for a bright near infrared (NIR) persistent luminescence signal centered on 700 nm (Supplementary Fig. S1.b and S1.c), which can be activated with either UV or orange-red irradiation. These optical properties are in total aggreement with previous results describing the optical behavior of Cr^{3+} in zinc gallate host[25,29]. Noteworthy regarding *in vivo* applications, persistent luminescence decay curves from Fig. S1.b, acquired over 30 minutes, clearly show the ability to retrieve a significant long-lasting NIR luminescence after a simple activation of the powder under the orange-red LEDs source. This signal, yet diminished compared to the one acquired after UV excitation, has already been proven to be largely sufficient to gain access to long-term optical imaging through living tissues, without any time constraints[25]. The extraction of monodisperse nanoparticles suspension, with a size distribution approximately centered on 85 nm (hydrodynamic diameter), was achieved by selective sedimentation in 5 mM NaOH with a global extraction yield comprised between 30 and 40%, depending on the grinding force and hydroxylation time (Table 1, hydrodynamic diameter). The resulting crude nanoparticles, referred to as ZGO-OH, diplayed a slighlty positive surface charge, very likely attributed to protonated Ga-OH groups decorating the crystals (Table 1, zeta potential). This suspension of ZGO-OH was reacted with 3-aminopropyltriethoxysilane (APTES) in DMF for 3 or 6 hours, in order to control the aminosilane layer thickness. Both types of amine-covered nanoparticles were then reacted with the same solution of N-hydroxysuccinimide activated 5 kDa polyethylene glycol in DMF to give birth to stealth ZGO-PEG (DMF/3h) and ZGO-PEG (DMF/6h) nanoparticles (Scheme 1).

The physico-chemical parameters from Table 1 confirm a significant increase of both nanoparticles hydrodynamic diameter and global surface charge after aminosilane condensation and formation of primary amine-terminated nanoparticles, referred to as ZGO-NH_2. Noteworthy, due to a critical

aggregation of amine-terminated nanoparticles in aqueous solutions, hydrodynamic diameter measurements were made in absolute ethanol, leading to stable suspensions of ZGO-NH_2 nanoparticles. After a 3 hours reaction with APTES, the hydrodynamic diameter of ZGO-NH_2 (DMF/3h) nanoparticles reaches the value of 100 nm, which is about 15 nm above the initial size of ZGO-OH nanoparticles, and keeps increasing for ZGO-NH_2 (DMF/6h) nanoparticles to the final value of 130 nm. This net increase in hydrodynamic diameter after aminosilane coupling is associated with a significant change in the global surface charge. The initial zeta potential of ZGO-OH nanoparticles switches from 20 mV to 40 mV after the reaction with APTES (Table 1), no matter how long the coupling reaction. Similar trends have already been observed with silicate-based persistent luminescence nanoparticles whose surface displayed comparable zeta potential values after aminosilane coupling[7], and are generally assumed to be the result of primary amine functions covering the probe, protonated at neutral pH. The addition of 5 kDa PEG on the nanoparticles ensures efficient masking of the global surface charge that shifts from the highly positive value of 40 mV to one characteristic of the neutral state, around 0 mV. Besides this significant change in surface charge, PEG grafting is responsible for a large increase of nanoparticles hydrodynamic diameter in 5% glucose solution. The ZGO-PEG (DMF/3h) nanoparticles are approximately 120 nm wide, which corresponds to an increase of 20 nm in comparison to the initial ZGO-NH_2 (DMF/3h) nanoparticles (Table 1). The differential between amine and PEG-grafted nanoparticles is even more pronounced in the case of ZGO-PEG (DMF/6h) nanoparticles whose hydrodynamic diameter almost reaches the value of 190 nm. When compared to the hydrodynamic diameter of ZGO-NH_2 (DMF/6h) nanoparticles, this result, which corresponds to a global increase of 60 nm after PEG grafting, is very certainly associated to a larger amount of PEG attached to the surface of the nanoparticles.

Additional information about the qualitative change associated with each functionalization step was reachable through Fourier Transform Infrared (FTIR) spectroscopy. Supplementary Fig. S2.a and S2.b show the FTIR spectra of each kind of nanoparticles. First, nonfunctionalized ZGO nanoparticles display two strong absorption bands around 570 cm^{-1} and 400 cm^{-1}, two weak bands at 1594 cm^{-1} and

1000 cm^{-1} and a broad and weak band around 3350 cm^{-1}. On the functionalized ZGO-NH_2 nanoparticles, the N-H stretching (3350 cm^{-1}) and bending (1580 cm^{-1}) are superimposed with two bands of ZGO, no matter which reaction time in DMF. The band at 2900 cm^{-1} can be identified as the C-H stretching and can be found on every functionalized nanoparticles. The bands at 1120 cm^{-1} and 1040 cm^{-1} were assigned to the Si-O stretching and are characteristic of the link between the nanoparticles and the aminosilane coating. When looking at the PEG-coated nanoparticles, the band at 1650 cm^{-1} was assigned to the C=O stretching vibration of the amide function and the bands at 1100 cm^{-1} and 1030 cm^{-1} to the C-O stretching of the PEG chain overlapping the Si-O stretching vibration. Altogether, these FTIR results are in total agreement with previous works from literature that report the functionalization of different nanoparticles and surfaces with either aminosilane[30] or PEG moieties.[31]

The optical characterization of ZGO nanoparticles with different surface states is shown in Supplementary Fig. S2.c-f. Interestingly, the data from persistent luminescence decay curves and persistence luminescence spectra show similar optical properties for each kind of ZGO nanoparticles, no matter which excitation source (red LEDs or UV light). This result suggests a poor influence of surface functionalization on persistent luminescence signal from these ZGO crystals. Noteworthy regarding the physico-chemical parameters reported above in the manuscript, all the hydrodynamic diameter values are associated with a polydispersity index largely below 0.1 which is highly in favor of monodisperse samples (Table 1). In addition, transmission electron microscopy (Supplementary Fig. S3.a-e) confirmed that the grafting of either aminosilane or PEG chain has no significant influence on the global morphology of the resulting ZGO nanoparticles. Unfortunately, classical physico-chemical characterization based on dynamic light scattering like hydrodynamic diameter and zeta potential measurements does not give any quantitative information in relation to the amount of aminosilane or PEG chains grafted after each functionalization step.

Quantitative evaluation of the amount of silane moieties and PEG chains was achieved by having recourse to thermogravimetric analysis (TGA). Given the high thermal stability of zinc gallate structure, progressive heating of our samples could lead to the effective decomposition of the organic layer,

grafted on the surface of the nanoparticles, without affecting the spinel core. The weight loss curves from Fig. 1 allow a clear differenciation of each funtionalization step. First, increasing the reaction time of ZGO-OH nanoparticles with APTES from 3 to 6 hours leads to a higher amount of aminosilane on the surface, attested by a significant increase in weight loss percentage evolving from 1.5 %, for ZGO-NH_2 (DMF/3h) nanoparticles, to the doubled value of 3 % in the case of ZGO-NH_2 (DMF/6h). Despite the same reaction conditions during PEG grafting, increasing the amount of aminosilane is responsible for a concomitant growth in the number of PEG chain. In the case of ZGO-PEG (DMF/3h) nanoparticles, the weight loss percentage stabilizes at 3.5 %, which represents less than half the value reached with ZGO-PEG (DMF/6h) nanoparticles of almost 8 % of total weight loss. Starting from the molecular weight of each grafted species, we were able to quantify the concentration of aminosilane and PEG moieties per mass unit of nanoparticles. Results from Table 2 indicate that a longer reaction time in APTES solution leads to a larger amount of aminosilane on the surface of ZGO-NH_2 nanoparticles. The concentration of silane increases from 60 nmol/mg, for ZGO-NH_2 (DMF/3h) nanoparticles, to 182 nmol/mg for ZGO-NH_2 (DMF/6h) nanoparticles. When the silane concentration is increased by a factor 3, the amount of PEG chain increases from 4 nmol/mg, for stealth nanoparticles synthesized from ZGO-NH_2 (DMF/3h), to almost 9 nmol/mg for ZGO-PEG (DMF/6h) nanoparticles (Table 2). Interestingly, the growth of a thick aminosilane layer highly contributes to the significant increase in PEG chain concentration, without affecting the grafting conditions, i.e without using higher concentration of PEG reagent or higher temperatures during the reaction.

Combining the results from physico-chemical techniques and TGA measurements gave access to an evaluation of the density of aminosilane and PEG chains per surface unit on a single nanoparticle. The calculation leans upon the hydrodynamic diameter of nanoparticles from the previous functionalization step and the approximation that each crystal is an exact sphere. As an example, the density of aminosilane grafted on a ZGO-OH nanoparticle after a 3 hours reaction with APTES was evaluated from the accessible surface on a ZGO-OH nanoparticle. The ATG-based aminosilane concentration, devided by the number of particles comprised in one mg of powder, gave the concentration of

aminosilane moieties per nanoparticle. This concentration normalized in relation to the total accessible surface on a ZGO-OH nanoparticle finally led to the density of aminosilanes per surface unit. The same protocol was adapted for the calculation of PEG density. When we compare the density of aminosilane grafted after 3 and 6 hours reaction in APTES, we notice a three times increase in the number of silane moieties increasing from 3 silane moieties/nm^2 on ZGO-NH_2 (DMF/3h) to more than 9 silane moieties/nm^2 on ZGO-NH_2 (DMF/6h), which is in total agreement with the concentration reported in Table 2. Surprisingly, the results from PEG density calculation follow a very different trend. The number of PEG moieties poorly increases from 0.15 to 0.19 PEG moieties/nm^2 for ZGO-PEG (DMF/3h) and ZGO-PEG (DMF/6h), respectively. Such 25 % increase in PEG density should be compared to the 225 % increase in PEG concentration, meaning that the global amount of PEG moieties per surface unit on the nanoparticle is almost left unchanged between ZGO-PEG (DMF/3h) and ZGO-PEG (DMF/6h). Pursuing the idea and recent observation that such difference in stealth nanoparticles surface states and physico-chemical characteristics could control the adsorption of serum proteins onto the surface of persistent luminescence nanoparticles and drastically change the "biological identity" of a crystal *in vivo*[12], we investigated the ability of these different nanoparticles to interact with serum protein *in vitro*. Each type of nanoparticles, chosen between ZGO-OH, ZGO-PEG (DMF/3h) and ZGO-PEG (DMF/6h), was first incubated for two hours at 37°C with 50% v/v mouse serum diluted in normal saline solution. After several washing steps, the amount and cartography of adsorbed proteins were then determined by combining the Bradford assay to a polyacrylamide gel electrophoresis. Results from the Bradford assay in Fig. 2.a show that PEG grafting is associated with a large decrease in the amount of adsorbed proteins. The global amount of protein per mg of nanoparticles was determined to be of 260 µg on ZGO-PEG (DMF/3h), which is relatively low in comparison to the 335 µg adsorbed per mg of ZGO-OH nanoparticles. This value keeps decreasing and reaches the minimum of 252 µg per mg for ZGO-PEG (DMF/6h) nanoparticles. This result, obtained from Bradford assay, was confirmed by running a polyacrylamide gel with the same samples (Fig. 2.b). We clearly notice a similar trend from the rapid observation of lanes distribution and intensity on the gel. In comparison to the control lane,

corresponding to 50% v/v mouse serum diluted in normal saline solution, we observe a progressive fainting of the 5 major bands between 39 and 64 kDa upon the addition of PEG on the surface of the nanoparticles. This trend was further analyzed with ImageJ software in order to precisely follow the evolution of the proteins cartography on the surface of ZGO nanoparticles. The analysis of lane profiles seems to indicate that PEG grafting is responsible for the elimination of the lightest proteins, attested by the complete disappearance of bands 4 and 5 in the two last lanes (Supplementary Fig. S4). Such result is in total agreement with the work of Chan et al. studying the adsorption of serum proteins on the surface of PEGylated gold nanoparticles[12]. Regarding both PEGylated nanoparticles, the more aminosilane moieties and the larger the nanoparticles, the fewer proteins adsorbed on their surface. Indeed, contrary to the cartography defined on ZGO-PEG (DMF/3h) nanoparticles, the third band does not appear in the lane associated to ZGO-PEG (DMF/6h) nanoparticles. These series of results from physico-chemical characterization as well as protein adsorption on both crude and PEGylated persistent luminescence nanoparticles strongly suggest that a significant increase of aminosilane density, along with a large augmentation of the hydrodynamic diameter, can successfully prevent the adsorption of proteins on the surface of stealth ZGO nanocrystals. Given the minor evolution of PEG density when comparing ZGO-PEG (DMF/3h) to ZGO-PEG (DMF/6h) nanoparticles, this general trend is most likely the result of progressive blockage of protein binding sites on the surface of the nanoparticles caused by the dense aminosilane corona surrounding the crystal core.

To fully understand the physiological implications of such adsorption patterns, we finally compared the behavior of these three different types of nanoparticles *in vivo*. Prior to systemic administration, each type of nanoparticles was first activated under UV light to allow real-time and dynamic detection of persistent luminescence signal right after the administration. Biodistribution of the probes was then continuously monitored for 30 minutes, and assessed after 1, 3 and 6 hours after LEDs activation. Persistent luminescence images, presented in Fig. 3.a, reveal a very different biodistribution pattern from one nanoparticles type to another. Crude ZGO-OH nanoparticles are almost instantly trapped within major organs of the mononuclear phagocyte system, which is assessed by a clear concentration of

the luminescence signal in liver and spleen. The main circulation routes remain completely extinguished, from the lower to the upper limb, and the images demonstrate no significant evolution of the biodistribution over the whole acquisition period. The biodistribution dynamics, recorded for the first 30 minutes and expressed as a percentage of the total luminescence signal retrieved within a region of interest (ROI) drawn around the major organs of the reticuloendothelial system (RES), are presented in Fig. 3.b. According to the semi quantitation from Fig. 3b, the accumulation process of ZGO-OH within liver and spleen is very fast and ends after 5 minutes, by which approximately 80 % of the nanoparticles remain trapped in the mononuclear phagocyte system. The same measurements after 1, 3, and 6 hours, displayed in Fig. 3.c, confirm this value, without any evolution of the biodistribution pattern. The results are largely different for both ZGO-PEG (DMF/3h) and ZGO-PEG (DMF/6h) nanoparticles. First, the images in Fig. 3.a indicate that stealth nanoparticles are predominantly able to remain in the main blood circulation, up to 3 hours for ZGO-PEG (DMF/3h) and up to 6 hours for ZGO-PEG (DMF/6h). We notice that PEG grafting allows a much better distribution of the probes within the animal body, bringing light to the upper and lower limbs circulation routes. When we compare the biodistribution of the two PEGylated crystals, we observe a longer circulation of the ZGO-PEG (DMF/6h) nanoparticles for which liver accumulation only appears 6 hours after the injection. In the case of ZGO-PEG (DMF/3h) nanoparticles, liver retention seems to be quicker and slowly evolves from 30 minutes to 3 hours, after which it becomes predominant. The semi-quantitation from persistent luminescence images (Fig. 3.b and c) confirms a slow and progressive accumulation of the stealth nanoparticles wihtin major RES organs. The 24 hours *ex vivo* biodistribution assessed the final utpake of all types of nanoparticles in both liver and spleen (Supplementary Fig. S5). The blood half-life of each type can be evaluated from the biodistribution data in Fig. 3 and evolves from 2-3 minutes, for crude nanoparticles, to 3 hours for ZGO-PEG (DMF/3h) nanoparticles and almost 6 hours for ZGO-PEG (DMF/6h) nanoparticles. Along with the results from physico-chemical characterization and protein adsorption, these biodistribution data demonstrate the important role of functionalization in defining the biological identity of the nanoparticles. Noteworthy, increasing the hydrodynamic diameter of stealth

persistent luminescence nanoparticles by growing a thick aminosilane layer seems to prevent serum protein adsorption *in vitro* and finally leads to a longer circulation of the probes *in vivo*, with blood half-lifes that almost reach 6 hours after the injection of nanoparticles 190 nm-wide. Altogether, the results from this study suggest a concomitant effect of the aminosilane and PEG moieties in the ability of the nanoparticles to prevent protein adsorption *in vitro* as well as liver retention *in vivo*. Noteworthy, the number of PEG moieties/nm² appears to be relatively similar between ZGO-PEG (DMF/3h) and ZGO-PEG (DMF/6h) nanoparticles, which would very likely account for the same PEG configuration. Unfortunately, the aminosilane coupling reaction in DMF was rather hard to control and longer reaction times were associated with the progressive formation of macroscopic silane aggregates that resulted in a complete loss of colloidal stability (data not shown).

Conclusion. We used persistent luminescence to better understand the influence of surface state and physico-chemical properties on the interaction of nanoparticles with serum proteins *in vitro* and their biological fate *in vivo*. Results demonstrate that surface charge and chemistry constitute the two major parameters ruling proteins adsorption on the nanoparticles. Indeed, masking charges and increasing the aminosilane density were both shown to prevent the interaction of proteins with the surface of nanoparticles. This biological identity of the crystal, defined by the amount and type of serum proteins adsorbed on its surface, was proven to govern the biodistribution of persistent luminescence nanoparticles *in vivo*. Most noteworthy, we were able to prove that, at the expense of a large increase of the nanoparticles hydrodynamic diameter, the larger the aminosilane thickness on the surface of the core, the longer the circulation of the probes *in vivo*. This result not only constitutes the first report of 190 nm-wide stealth persistent luminescence nanoparticles with a blood half-life as high as 6 hours *in vivo*, but should also open exciting perspectives regarding the use of such nanotechnology for multiple diagnostics applications *in vivo* such as tumor targeting.

ACKNOWLEDGMENT. We thank René Lai-Kuen and Bruno Saubamea (Cellular and Molecular Imaging Platform, CRP2 - UMS 3612 CNRS - US25 Inserm-IRD - Université Paris Descartes), Bruno Viana (IRCP, CNRS UMR8247) and Johanne Seguin for their help performing TEM, persistent luminescence emission spectra and PAGE analysis as well as Bradford tests. This work has been supported by the French National Agency (ANR) in the frame of its program in Nanosciences and Nanotechnologies (NATLURIM project n°ANR-08-NANO-025).

SUPPORTING INFORMATION AVAILABLE. Experimental procedures, physical characteristics of ZGO nanoparticles, information regarding polyacrylamide gel electrophoresis analysis with ImageJ software as well as 24 hours *ex vivo* biodistribution of ZGO-PEG nanoparticles are provided as supplementary material.

FIGURE CAPTIONS.

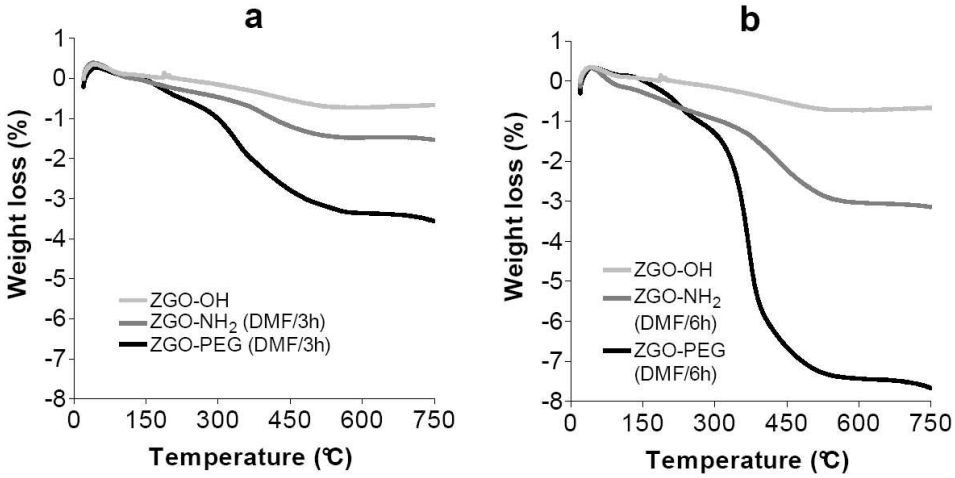

Figure 1. Weight loss curves obtained from thermogravimetric analysis of ZGO nanoparticles after each functionalization step. **a**, Functionalization route from aminosilanization in DMF for 3h. **b**, Functionalization route from aminosilanization in DMF for 6h.

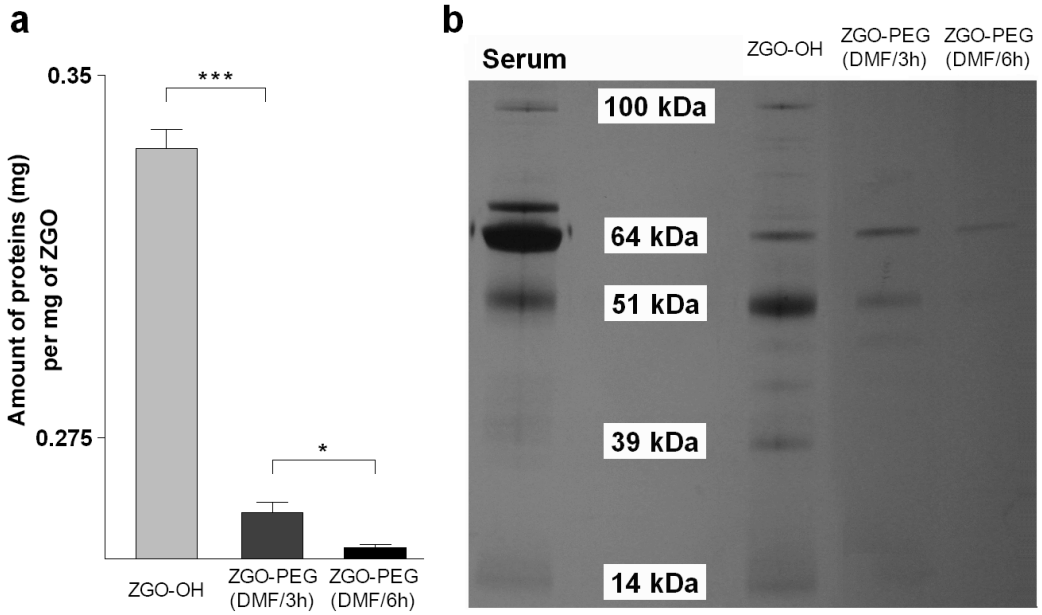

Figure 2. Interaction of ZGO nanoparticles with mouse serum proteins depending on surface coverage. **a**, Bradford assay after a 2 hours incubation of nanoparticles with mouse serum proteins. **b**, Polyacrylamide gel electrophoresis of proteins adsorbed on the surface of persistent luminescence nanoparticles.

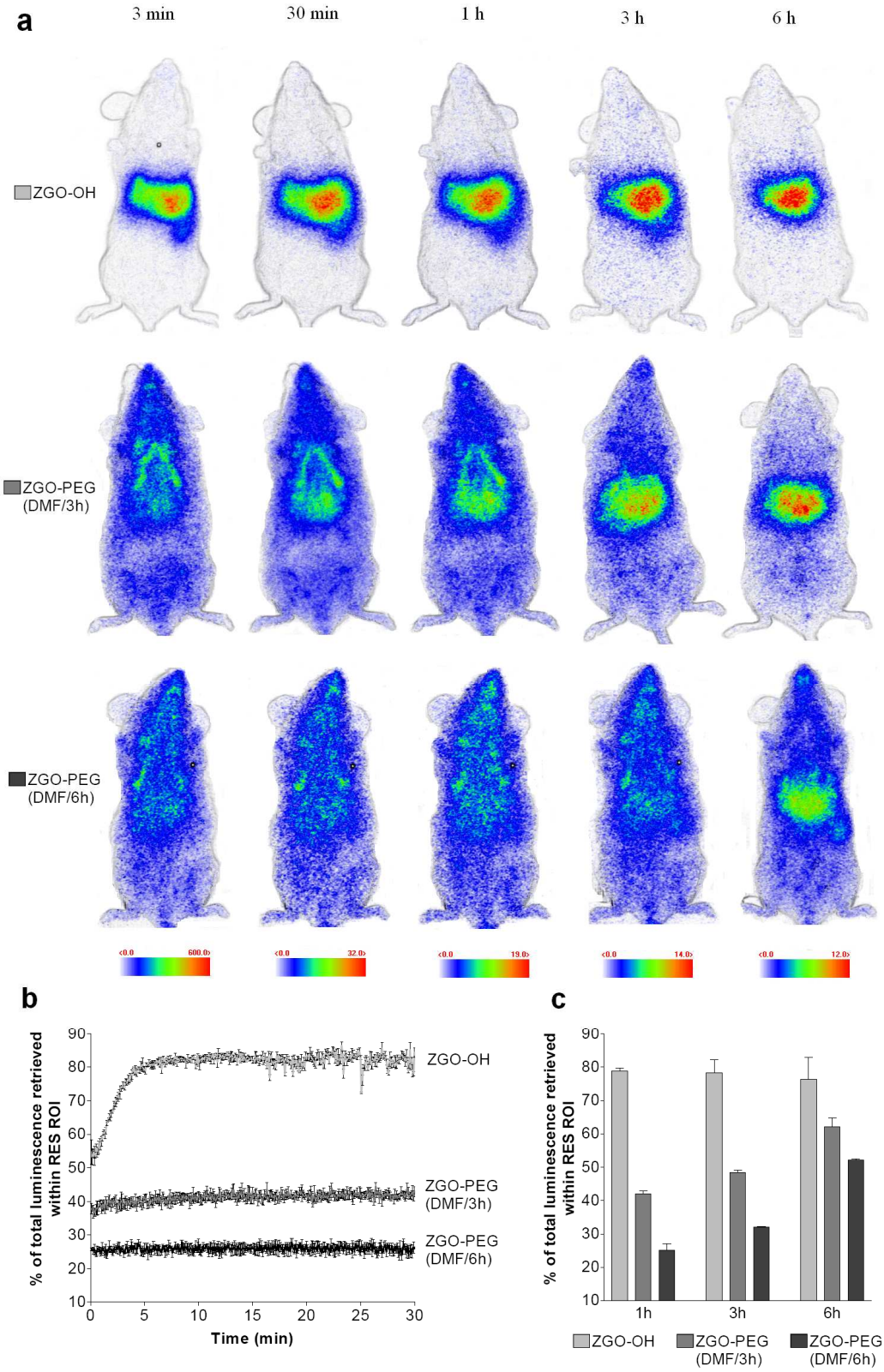

Figure 3. In vivo biodistribution of ZGO-PEG nanoparticles (n = 3). **a**, Persistent luminescence images of ZGO-PEG biodistribution. **b**, Accumulation kinetics of ZGO-PEG nanoparticles within RES ROI the first 30 minutes. **c**, Evolution of persistent luminescence signal within RES ROI after 1, 3 and 6 hours.

SCHEME TITLES.

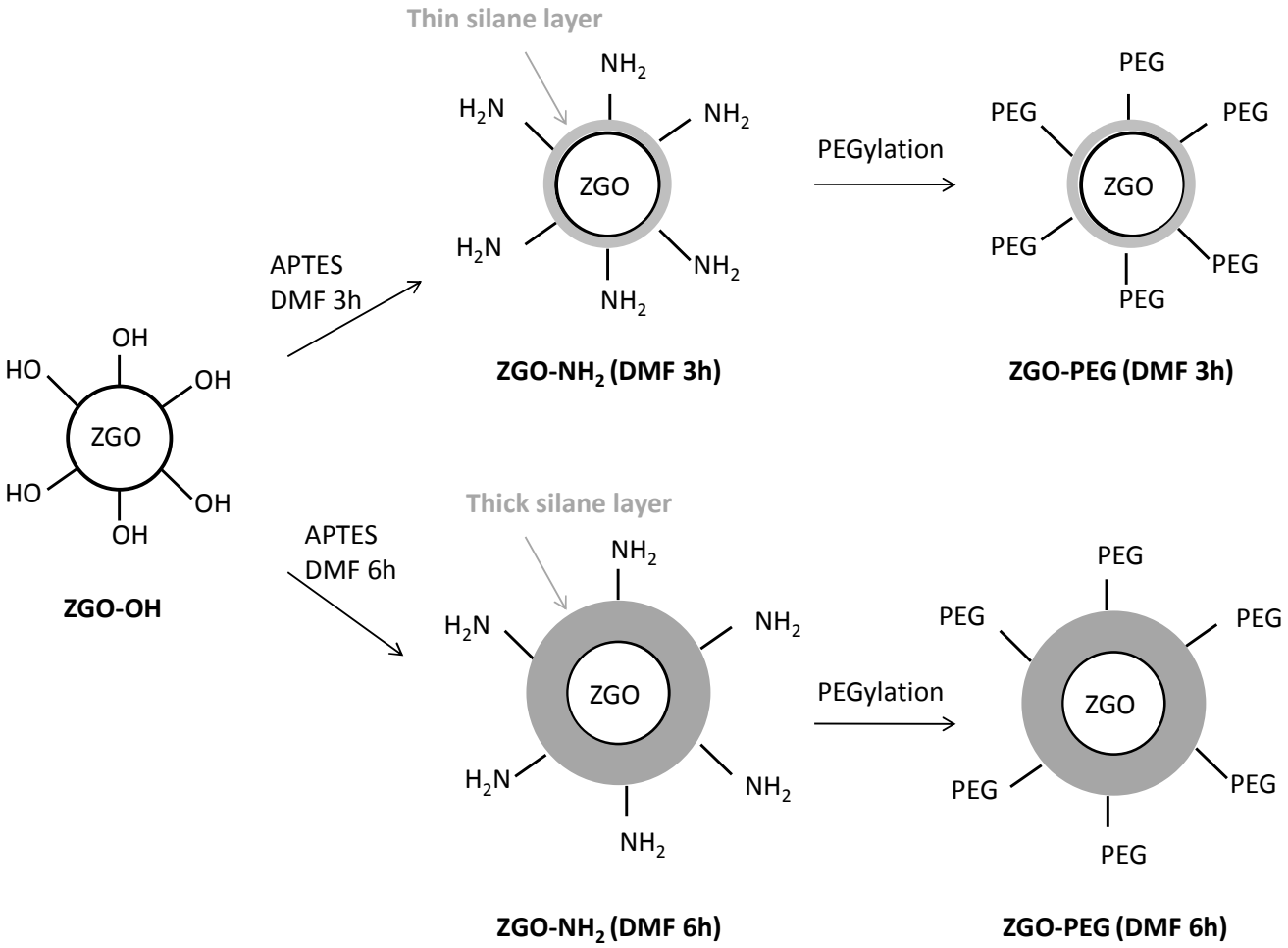

Scheme 1. Representation of ZGO functionalization routes.

TABLES.

	Hydrodynamic diameter (nm)	PDI	Zeta potential (mV)
ZGO-OH	84,52 ± 1,24	0.078 ± 0.018	22,2 ± 1,32
ZGO-NH_2 (DMF/3h)	99.02 ± 0.50	0.064 ± 0.008	39 ± 2.49
ZGO-NH_2 (DMF/6h)	133,10 ± 1,28	0.085 ± 0.035	40,7 ± 2,35
ZGO-PEG (DMF/3h)	122.90 ± 0.91	0.072 ± 0.014	2.04 ± 2.35
ZGO-PEG (DMF/6h)	188,10 ± 0,95	0.058 ± 0.02	- 0,37 ± 0,58

Table 1. Physico-chemical characterization of ZGO nanoparticles after each functionalization step.

	Silane concentration (nmol/mg)	PEG concentration (nmol/mg)
ZGO-NH_2 (DMF/3h)	60,87 ± 1,89	-

ZGO-NH_2 (DMF/6h)	182,55 ± 2,41	-
ZGO-PEG (DMF/3h)	-	3,92 ± 0,06
ZGO-PEG (DMF/6h)	-	8,89 ± 0,06

Table 2. Quantization of aminosilane and PEG density on ZGO nanoparticles from thermogravimetric analysis. Results are expressed as molar concentration per milligram of ZGO nanoparticles.

GRAPHICAL TABLE OF CONTENTS.

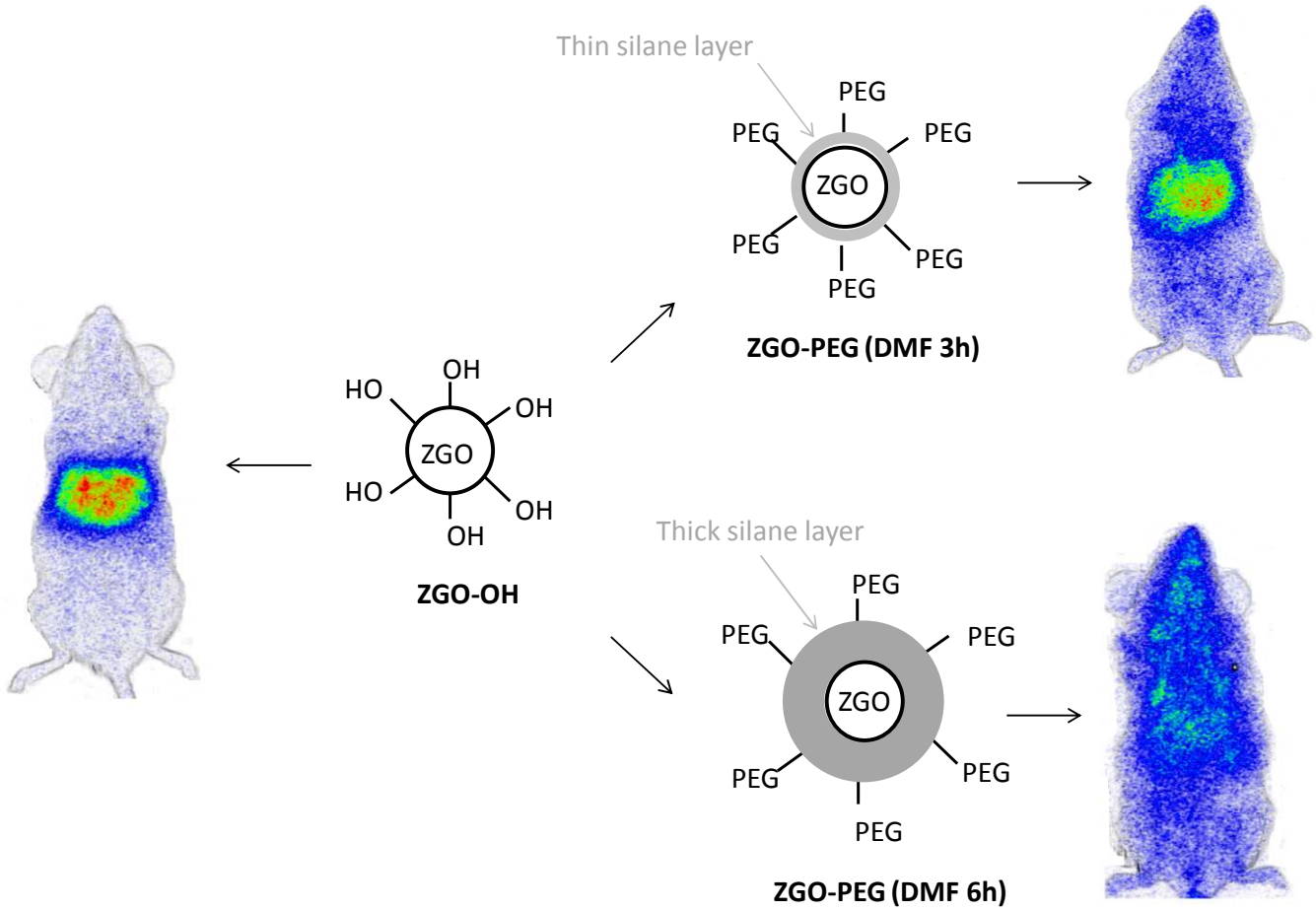

REFERENCES.

[1] Peer, D.; Karp, J.M.; Hong, S.; Farokhzad, O.C.; Margalit, R.; Langer, R. Nanocarriers as an emerging platform for cancer therapy. *Nat. Nanotechnol.* **2007,** 2(12), 751-60.

[2] Lin, X.; Xie, J.; Niu, G.; Zhang, F.; Gao, H.; Yang, M.; Quan, Q.; Aronova, M.A.; Zhang, G.; Lee, S.; Leapman, R.; Chen, X. Chimeric Ferritin Nanocages for Multiple Function Loading and Multimodal Imaging. *Nano Lett.* **2011,** 11(2), 814-9.

[3] Petros, R.A.; DeSimone, J.M. Strategies in the design of nanoparticles for therapeutic applications. *Nat. Rev. Drug. Discov.* **2010,** 9(8), 615-27.

[4] Walczyk, D.; Bombelli, F.B.; Monopoli, M.P.; Lynch, I.; Dawson, K.A. What the Cell "Sees" in Bionanoscience. *J. Am. Chem. Soc.* **2010,** 132(16), 5761-8.

[5] Park, J.H.; Gu, L.; von Maltzahn, G.; Ruoslahti, E.; Bhatia, S.N.; Sailor, M.J. Biodegradable luminescent porous silicon nanoparticle for in vivo applications. *Nat. Mater.* **2009,** 8(4), 331-6.

[6] Li, S.D. ; Huang, L. Pharmacokinetics and Biodistribution of Nanoparticles. *Mol. Pharm.* **2008,** 5(4), 496-504.

[7] le Masne de Chermont, Q.; Chanéac, C.; Seguin, J.; Pellé, F.; Maîtrejean, S.; Jolivet, J.P.; Gourier, D.; Bessodes, M.; Scherman, D. Nanoprobes with near-infrared persistent luminescence for in vivo imaging. *Proc. Natl. Acad. Sci. U S A.* **2007,** 104(22), 9266-71.

[8] Cedervall, T.; Lynch, I.; Lindman, S.; Berggård, T.; Thulin, E.; Nilsson, H.; Dawson, K.A.; Linse, S. Understanding the nanoparticle–protein corona using methods to quantify exchange rates and affinities of proteins for nanoparticles. *Proc. Natl. Acad. Sci. U S A.* **2007,** 104(7), 2050-5.

[9] Tenzer, S.; Docter, D.; Rosfa, S.; Wlodarski, A.; Kuharev, J.; Rekik, A.; Knauer, S.K.; Bantz, C.; Nawroth, T.; Bier, C.; Sirirattanapan, J.; Mann, W.; Treuel, L.; Zellner, R.; Maskos, M.; Schild,

H.; Stauber, R.H. Nanoparticle Size Is a Critical Physicochemical Determinant of the Human Blood Plasma Corona, A Comprehensive Quantitative Proteomic Analysis. *ACS Nano.* **2011,** 5(9), 7155-67.

[10] Monopoli, M.P.; Walczyk, D.; Campbell, A.; Elia, G.; Lynch, I.; Bombelli, F.B.; Dawson, K.A. Physical-Chemical Aspects of Protein Corona Relevance to in Vitro and in Vivo Biological Impacts of Nanoparticles. *J. Am. Chem. Soc.* **2011,** 133(8), 2525-34.

[11] Jeon, S.I.; Lee, J.H.; Andrade, J.D.; De Gennes, P.G. Protein-surface interactions in the presence of polyethylene oxide: I. Simplified theory. *J. Colloid Interface Sci.* **1991,** 142(1), 149-158.

[12] Walkey, C.D.; Olsen, J.B.; Guo, H.; Emili, A.; Chan, W.C. Nanoparticle Size and Surface Chemistry Determine Serum Protein Adsorption and Macrophage Uptake. *J. Am. Chem. Soc.* **2012,** 134(4), 2139-47.

[13] Daou, T.J.; Li, L.; Reiss, P.; Josserand, V.; Texier, I. Effect of Poly(ethylene glycol) Length on the in Vivo Behavior of Coated Quantum Dots. *Langmuir.* **2009,** 25(5), 3040-4.

[14] Perry, J. L.; Reuter, K. G.; Kai, M. P.; Kevin P. Herlihy, Jones, S. W.; Chris Luft, J.; Napier, M.; Bear, J. E.; DeSimone J. M. PEGylated PRINT Nanoparticles: The Impact of PEG Density on Protein Binding, Macrophage Association, Biodistribution, and Pharmacokinetics. *Nano Letters* **2012**, 12, 5304-5310.

[15] Torrisi, V.; Graillot, A.; Vitorazi, L.; Crouzet, Q. ; Marletta, G.; Loubat, C.; Berret, J.F. Preventing corona effects: multiphosphonic acid poly(ethylene glycol) copolymers for stable stealth iron oxide nanoparticles. *Biomacromolecules*. **2014**, 15(8):3171-9.

[16] Huang, X.; Li, L.; Liu, T.; Hao, N.; Liu, H.; Chen, D.; Tang, F. The Shape Effect of Mesoporous Silica Nanoparticles on Biodistribution, Clearance, and Biocompatibility in Vivo. *ACS Nano.* **2011,** 5(7), 5390-9.

[17] Xiao, K.; Li, Y.; Luo, J.; Lee, J.S.; Xiao, W.; Gonik, A.M.; Agarwal, R.G.; Lam, K.S. The effect of surface charge on in vivo biodistribution of PEG-oligocholic acid based micellar nanoparticles. *Biomaterials.* **2011,** 32(13), 3435-46.

[18] Pombo García, K.; Zarschler, K.; Barbaro, L.; Barreto, J.A.; O'Malley, W.; Spiccia, L.; Stephan, H.; Graham, B. Zwitterionic-coated "stealth" nanoparticles for biomedical applications: recent advances in countering biomolecular corona formation and uptake by the mononuclear phagocyte system. Small. **2014**, 10(13):2516-29.

[19] Poon, Z.; Lee, J.B.; Morton, S.W.; Hammond, P.T. Controlling in Vivo Stability and Biodistribution in Electrostatically Assembled Nanoparticles for Systemic Delivery. *Nano Lett.* **2011,** 11(5), 2096-103.

[20] Maldiney, T.; Sraiki, G.; Viana, B.; Gourier, D.; Richard, C.; Scherman, D.; Bessodes, M.; Van den Eeckhout, K.; Poelman, D.; Smet, P.F. In vivo optical imaging with rare earth doped $Ca_2Si_5N_8$ persistent luminescence nanoparticles. *Opt. Mater. Express.* **2012,** 2(3), 261-8.

[21] Maldiney, T.; Byk, G.; Wattier, N.; Seguin, J.; Khandadash, R.; Bessodes, M.; Richard, C.; Scherman, D. Synthesis and functionalization of persistent luminescence nanoparticles with small molecules and evaluation of their targeting ability. *Int. J. Pharm.* **2012,** 423(1), 102-7.

[22] Maldiney, T.; Kaikkonen, M.U.; Seguin, J.; le Masne de Chermont, Q.; Bessodes, M.; Airenne, K.J.; Ylä-Herttuala, S.; Scherman, D.; Richard, C. In vitro targeting of avidin-expressing glioma cells with biotinylated persistent luminescence nanoparticles. *Bioconjug. Chem.* **2012,** 23(3), 472-8.

[23] Maldiney, T.; Richard, C.; Seguin, J.; Wattier, N.; Bessodes, M.; Scherman, D. Effect of core diameter, surface coating, and PEG chain length on the biodistribution of persistent luminescence nanoparticles in mice. *ACS Nano.* **2011,** 5(2), 854-62.

[24] Maldiney, T.; Lecointre, A.; Viana, B.; Bessière, A.; Bessodes, M.; Gourier, D.; Richard, C.; Scherman, D. Controlling electron trap depth to enhance optical properties of persistent luminescence nanoparticles for in vivo imaging. *J. Am. Chem. Soc.* **2011,** 133(30), 11810-5

[25] Maldiney, T.; Bessière, A.; Seguin, J.; Teston, E.; Sharma, S.K.; Viana, B.; Bos, A.J.; Dorenbos, P.; Bessodes, M.; Gourier, D.; Scherman, D.; Richard, C. The in vivo activation of persistent nanophosphors for optical imaging of vascularization, tumours and grafted cells. *Nat. Mater.* **2014,** 13(4), 418-426.

[26] Maldiney, T.; Ballet, B.; Bessodes, M.; Scherman, D.; Richard, C. Mesoporous persistent nanophosphors for in vivo optical bioimaging and drug-delivery. Nanoscale. 2014, 6(22):13970-6.

[27] Teston, E.; Lalatonne, Y.; Elgrabli, D.; Autret, G.; Motte, L.; Gazeau, F.; Scherman, D.; Clément, O.; Richard, C.; Maldiney, T. Design, Properties, and In Vivo Behavior of Super-paramagnetic Persistent Luminescence Nanohybrids. Small. **2015**, doi:10.1002/smll.201403071.

[28] Maldiney, T.; Doan, B.-T.; Alloyeau, D.; Bessodes, M.; Scherman, D. and Richard, C. Gadolinium-Doped Persistent Nanophosphors as Versatile Tool for Multimodal In Vivo Imaging. Adv. Funct. Mater. 2015, 25(2): 331–338

[29] Bessière, A.; Jacquart, S.; Priolkar, K.; Lecointre, A.; Viana, B.; Gourier, D. $ZnGa_2O_4:Cr^{3+}$:a new red long-lasting phosphor with high brightness. *Opt Express.* **2011,** 19(11), 10131-7.

[30] Li, S.; Ma, W.; Zhou, Y.; Chen, X.; Ma, M.; Xu, Y. 3-aminopropyltriethoxysilanes Modified Porous Silicon as a Voltammetric Sensor for Determination of Silver Ion. *Int. J. Electrochem. Sci.* **2013,** 8,1802-1812.

[31] Devouge, S.; Conti, J.; Goldsztein, A.sztGosselin, E.eliBrans, A.sl Voue, M.eliDe Coninck, J.; Homble, F.; Goormaghtigh, E.; Marchand-Brynaert, J. Surface functionalization of germanium ATR devices for use in FTIR-biosensors. *J. Colloid Interf. Sci.* **2009**, 332, 2, 408-415.